



## Investigation of Ethanol Electro-Oxidation on a Pt–Sn–Co/C Catalyst for a Membraneless Ethanol Fuel Cell

S.P.R. Kalaikathir<sup>1</sup> and S. Begila David<sup>2\*</sup>

<sup>1</sup> Department of Chemistry, Womens' Christian College, Nagercoil – 629 001, India.

<sup>2</sup> PG and Research Centre in Chemistry, Scott Christian College (Autonomous), Nagercoil – 629 003, India.

**Abstract :** In the present work, carbon-supported, well-dispersed Pt<sub>100</sub>, Pt<sub>50</sub>Sn<sub>50</sub>, Pt<sub>50</sub>Co<sub>50</sub>, Pt<sub>60</sub>Sn<sub>30</sub>Co<sub>10</sub>, Pt<sub>60</sub>Sn<sub>20</sub>Co<sub>20</sub>, and Pt<sub>60</sub>Sn<sub>10</sub>Co<sub>30</sub> electrocatalysts were synthesized by Pechini method. The crystallite size, lattice parameter, composition, and particle size of metals in the electrocatalysts were determined by XRD, EDX and TEM techniques, respectively. X-ray diffraction analysis showed that catalysts have a Pt face-centred cubic (fcc) structure with crystallite size of 3–4.5 nm. The EDX results of the binary Pt–Sn/C and Pt–Co/C and the ternary Pt–Sn–Co/C catalysts were extremely close to the nominal values, indicating that the metals were loaded onto the carbon support without any obvious loss. The size of catalyst nanoparticles was observed via TEM and showed an average diameter of 3.1 nm. The electrocatalytic activities of Pt<sub>100</sub>/C, Pt<sub>50</sub>Sn<sub>50</sub>/C, Pt<sub>50</sub>Co<sub>50</sub>/C, Pt<sub>60</sub>Sn<sub>30</sub>Co<sub>10</sub>/C, Pt<sub>60</sub>Sn<sub>20</sub>Co<sub>20</sub>/C, and Pt<sub>60</sub>Sn<sub>10</sub>Co<sub>30</sub>/C catalysts were investigated in terms of CV and CA. The electrochemical results showed that the catalytic activity in 1.0 M EtOH + 0.5 M H<sub>2</sub>SO<sub>4</sub> solution at 0.5 V vs. Ag/AgCl exhibits the following sequence: Pt<sub>60</sub>Sn<sub>30</sub>Co<sub>10</sub>/C > Pt<sub>60</sub>Sn<sub>20</sub>Co<sub>20</sub>/C > Pt<sub>60</sub>Sn<sub>10</sub>Co<sub>30</sub>/C > Pt<sub>50</sub>Sn<sub>50</sub>/C > Pt/C > Pt<sub>50</sub>Co<sub>50</sub>/C. This clearly indicates that the performance of the ternary Pt<sub>60</sub>Sn<sub>30</sub>Co<sub>10</sub>/C electrocatalysts for ethanol electro-oxidation is better than that of the binary Pt<sub>50</sub>Sn<sub>50</sub>/C and Pt<sub>50</sub>Co<sub>50</sub>/C electrocatalysts due to the promoting function of Co. In addition, its CO-tolerance is better than that of the Pt<sub>50</sub>Ru<sub>50</sub>/C and Pt<sub>50</sub>Co<sub>50</sub>/C catalysts. The high activity of Pt<sub>60</sub>Ru<sub>30</sub>Co<sub>10</sub>/C electrocatalyst was also observed on membraneless ethanol fuel cell, which was consistent with the half-cell measurements.

**Keywords:** Membraneless ethanol fuel cell, Platinum, Cobalt, Tin, and Electrocatalysts.

### 1. Introduction

The development of the membraneless ethanol fuel cell (MLEFC) has been the target of many researchers, because ethanol is a liquid fuel which can be easily stored, handled and produced in large quantity from biomass through a fermentation process<sup>1-8</sup>. Despite all efforts devoted to the MLEFC development, there still remain problems in terms of efficiency and power density due to slow kinetics of the ethanol oxidation reaction at the anode will leads to high overpotentials.

Pt is known to activate the dissociative adsorption of ethanol at an appreciable rate. The main problem is that ethanol oxidation at a platinum electrode is a self-poisoning reaction, since strongly adsorbed CO and CH<sub>3</sub>COOH are produced by electrooxidation of ethanol<sup>9-11</sup>. To promote the ethanol electrooxidation at platinum, modification of the catalyst surface has been made by the addition of a second metal to platinum<sup>12-14</sup>.

The Pt–Sn/C binary metallic catalyst is commonly accepted as the best electrocatalyst for ethanol oxidation due to its high CO tolerance, which can be achieved via its electronic effects and bifunctional mechanisms<sup>15-16</sup> that improve the catalytic activities of electrochemical reactions. However, controversy exists concerning the real improvement of the ethanol electrooxidation reaction. Despite the controversies, recent studies have shown that the Pt–Sn–Co/C<sup>17-18</sup> catalyst has a dramatic effect on its electrocatalytic activity. The

enhanced activity of the ternary catalyst is due to the promoting effect of the second or third elements added to Pt. In the present study, we evaluated the catalytic activity for ethanol oxidation reaction (EOR) by incorporating Co into Pt–Sn/C catalysts in MLEFC.

## 2 Experimental

### 2.1 Materials

The metal precursors used for the preparation of electrocatalysts were  $\text{H}_2\text{PtCl}_6 \cdot 6\text{H}_2\text{O}$  (from Sigma Aldrich),  $\text{SnCl}_2 \cdot 2\text{H}_2\text{O}$  (from Sigma Aldrich), and  $\text{Co}(\text{NO}_3)_2 \cdot 6\text{H}_2\text{O}$  (from Sigma Aldrich). Vulcan XC-72R carbon black (from Cabot Corp.) was used as a support for the catalysts. Graphite plates (from E-TEK) were used as substrates for the catalyst to prepare the electrodes. Ethylene glycol (from Merck) was used as the solvent and reduction agent. Nafion<sup>®</sup> (DE 521, DuPont USA) dispersion was used to make the catalyst ink. Ethanol (from Merck), sodium perborate (from Riedel),  $\text{H}_2\text{SO}_4$  (from Merck) and sea water were used as the fuel, the oxidant and as the electrolyte for electrochemical analysis, respectively. All the chemicals were of analytical grade. Pt/C (40-wt%, from E-TEK) was used as the cathode catalyst.

### 2.2 Catalyst Preparation

Carbon-supported catalysts containing Pt, Sn and Co with different atomic ratios were synthesized employing ethylene glycol (EG) as a reactant and reducing agent together with citric acid (CA) in line with the Pechini methodology<sup>19-21</sup>. The Pt, Sn and Co precursors were prepared separately by employing metallic salts, namely,  $\text{H}_2\text{PtCl}_6 \cdot 6\text{H}_2\text{O}$ ,  $\text{SnCl}_2 \cdot 2\text{H}_2\text{O}$  and  $\text{Co}(\text{NO}_3)_2 \cdot 6\text{H}_2\text{O}$ , dissolved in a mixture of EG and CA at 70 °C and the mixture was kept under vigorous stirring for 2–3 h composing a polyester network that contains the metallic ions homogeneously distributed. The CA/EG/metal molar ratio is 4:16:1 for all the polymeric precursors. It appears that the citric chelate helps to prevent particle aggregation in a certain extent and induce nanoparticles to get high dispersion.

To obtain the supported catalysts, appropriate amounts of the polymeric precursors were dissolved in ethanol and a calculated amount of the functionalized carbon black support was added. Finally, the mixture precursor solution/carbon was homogenized in an ultrasonic bath and then calcinated at different temperatures under an air atmosphere, using a temperature program reaching 400 °C to eliminate the excess carbon<sup>22</sup>. For comparison, the monometallic Pt/C, and bimetallic Pt–Sn/C and Pt–Co/C catalysts were synthesized under the same conditions. The electrocatalytic mixtures and atomic ratios were  $\text{Pt}_{60}\text{Sn}_{30}\text{Co}_{10}/\text{C}$ ,  $\text{Pt}_{60}\text{Sn}_{20}\text{Co}_{20}/\text{C}$ ,  $\text{Pt}_{60}\text{Sn}_{10}\text{Co}_{30}/\text{C}$ ,  $\text{Pt}_{50}\text{Sn}_{50}/\text{C}$ ,  $\text{Pt}_{50}\text{Co}_{50}/\text{C}$  and  $\text{Pt}_{100}/\text{C}$ . The nominal loading of metals in the electrocatalysts was 40 %wt and rest 60 %wt was carbon.

## 3 Results and discussions

### 3.1 Physical characterization

#### 3.1.1 X-ray diffraction (XRD)

The XRD patterns of the prepared  $\text{Pt}_{60}\text{Sn}_{30}\text{Co}_{10}/\text{C}$ ,  $\text{Pt}_{60}\text{Sn}_{20}\text{Co}_{20}/\text{C}$ ,  $\text{Pt}_{60}\text{Sn}_{10}\text{Co}_{30}/\text{C}$ ,  $\text{Pt}_{50}\text{Sn}_{50}/\text{C}$ ,  $\text{Pt}_{50}\text{Co}_{50}/\text{C}$  and  $\text{Pt}_{100}/\text{C}$  catalysts are shown in Fig. 1.

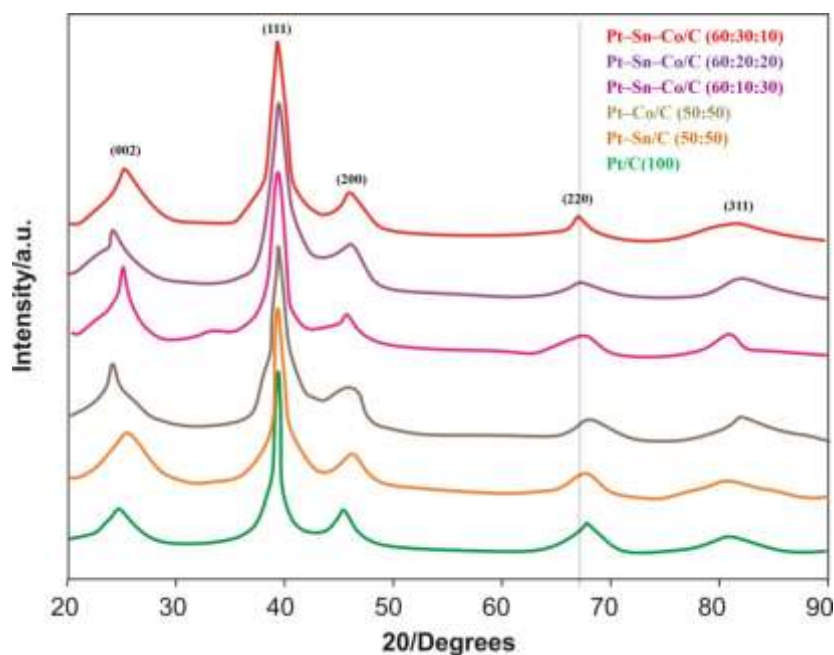


**Fig. 1** X-ray diffraction patterns of  $\text{Pt}_{60}\text{Sn}_{30}\text{Co}_{10}/\text{C}$ ,  $\text{Pt}_{60}\text{Sn}_{20}\text{Co}_{20}/\text{C}$ ,  $\text{Pt}_{60}\text{Sn}_{10}\text{Co}_{30}/\text{C}$ ,  $\text{Pt}_{50}\text{Sn}_{50}/\text{C}$ ,  $\text{Pt}_{50}\text{Co}_{50}/\text{C}$  and  $\text{Pt}_{100}/\text{C}$  catalysts

The first peak located at around  $25^\circ$  in all the XRD patterns is attributable to the Vulcan XC-72R carbon support. The  $2\theta$  of the (2 2 0) peak for  $\text{Pt}_{60}\text{Sn}_{30}\text{Co}_{10}/\text{C}$ ,  $\text{Pt}_{60}\text{Sn}_{20}\text{Co}_{20}/\text{C}$ ,  $\text{Pt}_{60}\text{Sn}_{10}\text{Co}_{30}/\text{C}$ ,  $\text{Pt}_{50}\text{Sn}_{50}/\text{C}$  and  $\text{Pt}_{50}\text{Co}_{50}/\text{C}$  shows a higher angle shift than the characteristics of face-centered cubic (fcc) crystalline Pt at  $2\theta$  values of  $38^\circ$ ,  $48^\circ$ ,  $67.5^\circ$  and  $83^\circ$  and are indexed with planes (1 1 1), (2 0 0), (2 2 0) and (3 1 1), respectively, indicating that the electrocatalysts have good alloy formations and suggesting the effect of a different atomic rate of Co in the ternary catalyst. No diffraction peaks were attributed to pure tin and cobalt or tin rich hexagonal close packed (hcp) phase, appear in the XRD patterns, suggesting that tin and cobalt atoms either form an alloy with platinum or exist as amorphous oxide phases. The Pt–Co/C electrocatalyst also showed the same characteristic peak as that of the Pt–Sn/C electrocatalysts.

The fcc lattice parameters were evaluated from the angular position of the (2 2 0) peaks, which reflect the formation of a solid solution (Table 1).

**Table 1** The EDX composition, lattice parameters, and the particle size obtained for different atomic ratios of electrocatalysts

Electrocatalyst	Nominal Atomic ratio			EDX Atomic ratio			Lattice parameter (nm)	Crystallite size (nm)	Particle size from TEM (nm)
	Pt	Sn	Co	Pt	Sn	Co			
Pt/C	100	-	-	99	-	-	0.3915	4.5	4.1
Pt–Co/C	50	-	50	52	-	48	0.3905	4.4	4.1
Pt–Sn/C	50	50	-	51	49	-	0.3887	3.9	3.6
Pt–Sn–Co/C	60	10	30	63	8	29	0.3904	3.7	3.4
Pt–Sn–Co/C	60	20	20	63	19	18	0.3896	3.5	3.3
Pt–Sn–Co/C	60	30	10	62	28	11	0.3899	3.2	3.1

The decrease in lattice parameters of the alloy catalysts reflects the progressive increase in the incorporation of Sn and Co into the alloyed state. The difference of lattice parameters and the shift of (2 2 0) plane indicate interactions between Pt, Sn and Co. The average particle size for Pt–Sn/C, Pt–Co/C, and Pt–Sn–Co/C electrocatalysts were in the range of 3–4.5 nm was estimated using the Scherrer equation.

### 3.1.2 Transmission Electron Microscopy (TEM)

TEM image of the Pt–Sn–Co/C alloy catalysts and the corresponding particle size distribution histogram are presented in Fig. 2.

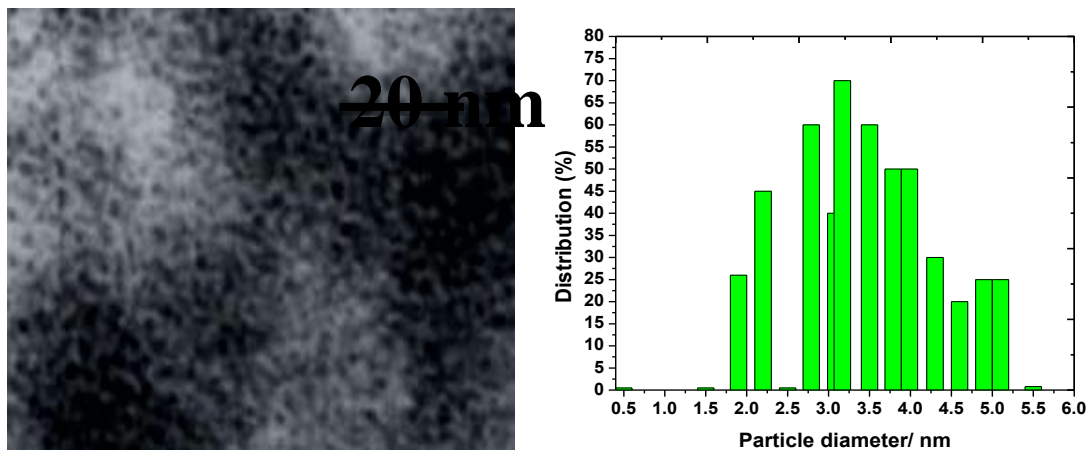
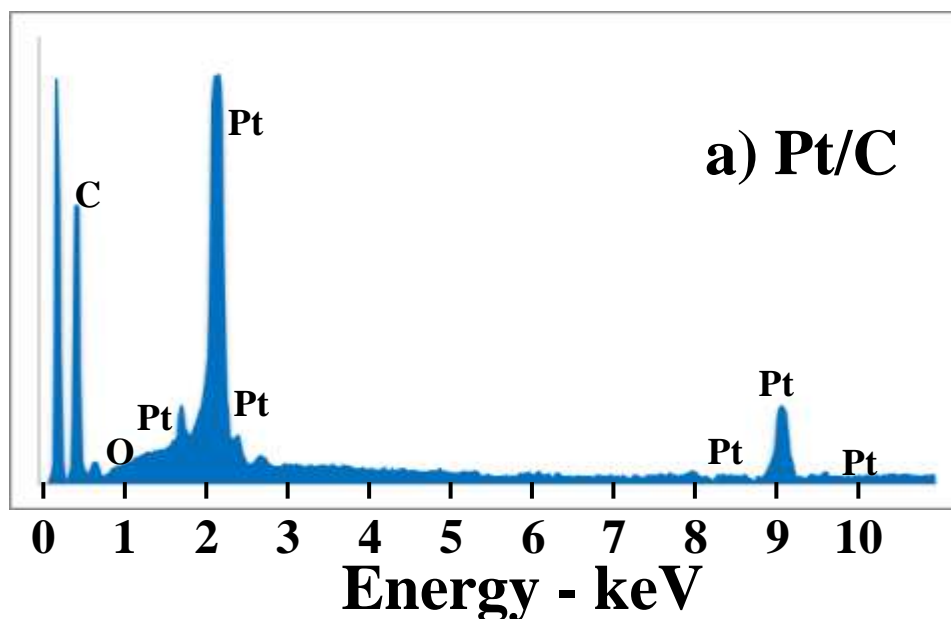


**Fig. 2** TEM image and particle size distribution of Pt–Sn–Co/C catalyst

From the TEM images, the average particle diameter was found to be approximately 3-4 nm, which is in fairly good agreement with the data calculated from XRD. The particle size distribution of these catalysts is shown in Table 1 in accordance to the TEM images.

### 3.1.3 Energy Dispersive X-ray Spectroscopy (EDX)

Energy dispersive X-ray spectroscopy is conducted by focusing the electron beam on several different selected regions of the carbon supported Pt–Sn–Co nanoparticles. An EDX spectrum of Pt–Sn–Co/C nanoparticle is shown in Fig. 3. The average composition of the sample was in atom ratio of Pt:Sn:Co = 6:3:1. The EDX results of the binary Pt–Sn/C and Pt–Co/C and the ternary Pt–Sn–Co/C catalysts are very close to the nominal values, which indicate that the metals were loaded onto the carbon support without obvious loss.



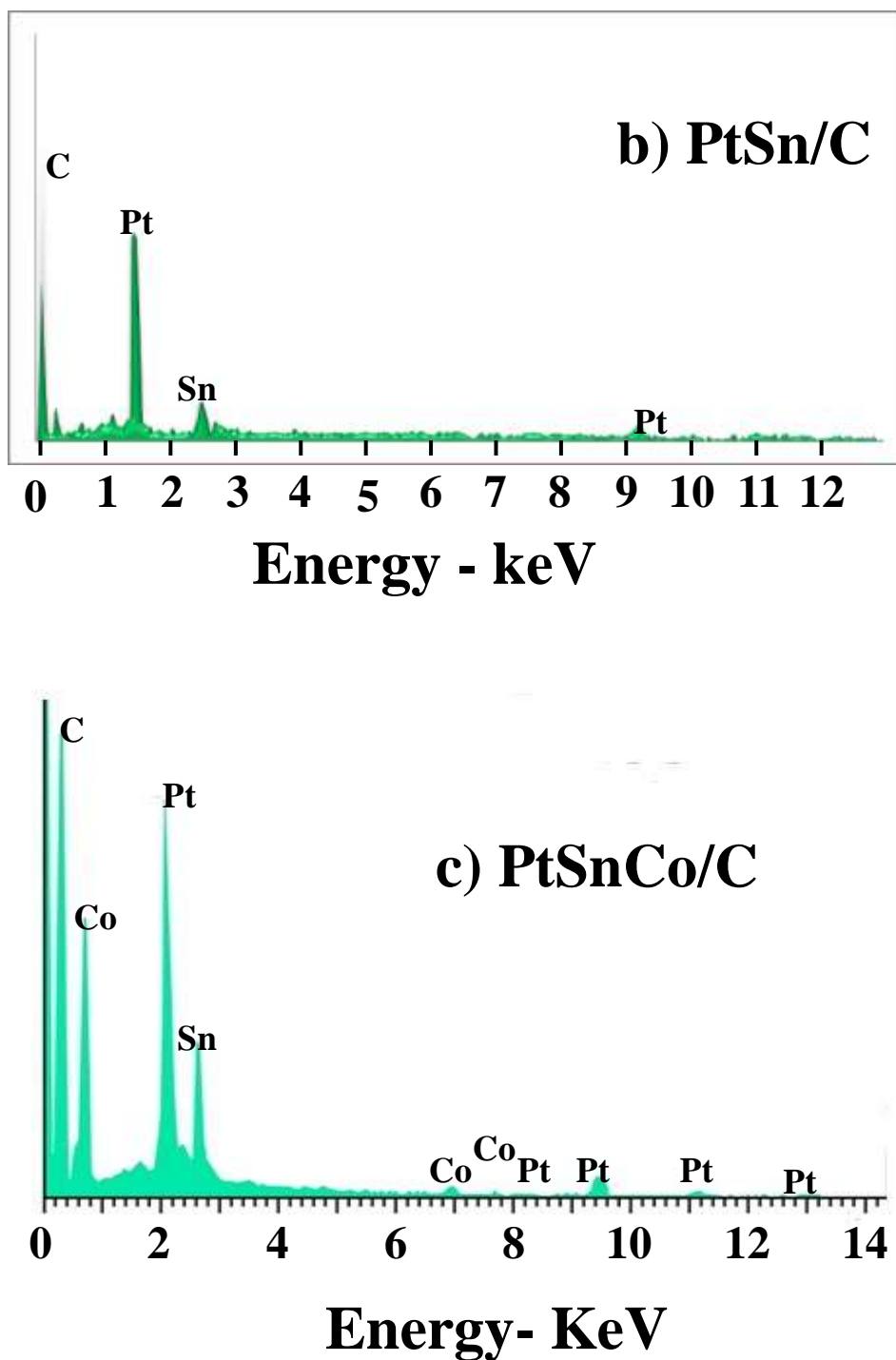
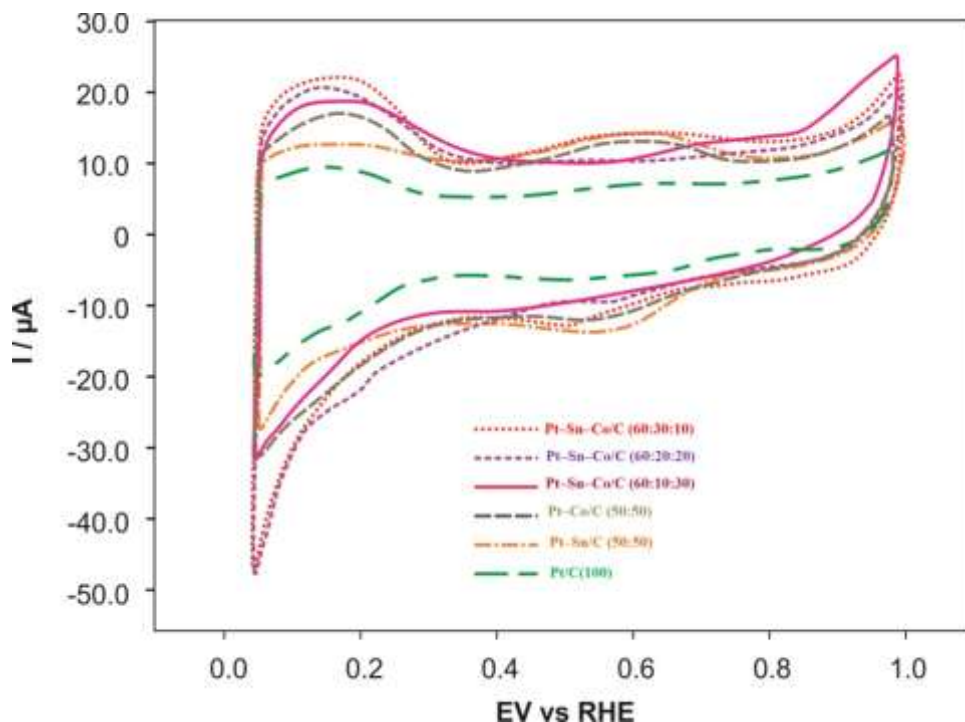


Fig. 3 EDX spectra of a) Pt/C, b) Pt–Sn/C and c) Pt–Sn–Co/C catalysts.

### 3.2 Electrochemical Characterization

#### 3.2.1 Cyclic Voltammetry

Fig. 4a shows the cyclic voltammogram (CV) on the Pt<sub>60</sub>Sn<sub>30</sub>Co<sub>10</sub>/C, Pt<sub>60</sub>Sn<sub>20</sub>Co<sub>20</sub>/C, Pt<sub>60</sub>Sn<sub>10</sub>Co<sub>30</sub>/C, Pt<sub>50</sub>Sn<sub>50</sub>/C, Pt<sub>50</sub>Co<sub>50</sub>/C and Pt<sub>100</sub>/C catalysts for CO oxidation in a solution of 0.5 M H<sub>2</sub>SO<sub>4</sub>. Due to the strong adsorption of CO onto the Pt surface, the hydrogen adsorption-desorption of the Pt was completely blocked in the hydrogen region; indicating the presence of a saturated CO adlayer<sup>23</sup>.



**Fig. 4a** CVs of  $\text{Pt}_{60}\text{Sn}_{30}\text{Co}_{10}/\text{C}$ ,  $\text{Pt}_{60}\text{Sn}_{20}\text{Co}_{20}/\text{C}$ ,  $\text{Pt}_{60}\text{Sn}_{10}\text{Co}_{30}/\text{C}$ ,  $\text{Pt}_{50}\text{Sn}_{50}/\text{C}$ ,  $\text{Pt}_{50}\text{Co}_{50}/\text{C}$  and  $\text{Pt}_{100}/\text{C}$  electrocatalysts in 0.5 M  $\text{H}_2\text{SO}_4$

In comparison to pure Pt, the oxidation of  $\text{CH}_3\text{CH}_2\text{OH}_{\text{ads}}$  at Co containing Pt–Sn/C surfaces exhibits a shift of the peak potential to lower potentials. The ethanol oxidation evokes a quick formation of  $\text{CO}_{\text{ads}}$  at very low potentials, where  $\text{CO}_{\text{ads}}$  is not yet oxidized, and so hinders the further adsorption and decomposition of ethanol. At potentials above the onset potential of the adsorbate oxidation, both parallel oxidation paths are taking place simultaneously. At a low potential, higher current efficiencies for  $\text{CO}_2$  are observed on Pt–Sn–Co/C electrodes than on pure Pt surfaces. This suggests that in presence of Co, Sn ad-atoms promote the reaction path *via*  $\text{CO}_{\text{ads}}$  in the low potential region. At higher potentials, the same current efficiency for  $\text{CO}_2$  as on pure Pt indicates that the ternary Pt–Sn–Co/C electrocatalysts loses its co-catalytic activity towards ethanol oxidation. This loss of the activity is possibly caused by the formation of inactive anhydrous Sn oxide at higher potentials. The CV curves were obtained in a half cell between 0.05 and 1.0 V (vs. Ag/AgCl) in the absence of ethanol. The characteristic features of polycrystalline Pt, i.e. hydrogen adsorption/desorption peaks in low potential region, oxide formation/stripping wave/peak in high potential region and a flat double layer in between, are observed for all the synthesized catalysts. The voltammograms of the electrocatalysts did not display a well-defined hydrogen region between 0.05 and 0.35 V, as the catalyst's features in this region are influenced by their surface composition.

Fig. 4b shows the cyclic voltammograms (CV) of ethanol oxidation under acidic conditions (1.0 M  $\text{C}_2\text{H}_5\text{OH}$  and 0.5 M  $\text{H}_2\text{SO}_4$ ) catalyzed by Pt–Sn/C (50:50), Pt–Co/C (50:50), Pt–Sn–Co/C (60:30:10), Pt–Sn–Co/C (60:20:20) and Pt–Sn–Co/C (60:10:30) catalysts. All the current values were normalized by the geometric surface area of the electrode used. There were three oxidation peaks when ethanol CV was carried out on the Pt/C catalyst (vs. Ag/AgCl), two during the forward scan and one during the reverse scan. The main results of CV test of Pt–Sn/C (50:50), Pt–Sn/C (50:50), Pt–Sn–Co/C (60:30:10), Pt–Sn–Co/C (60:20:10) and Pt–Sn–Co/C (60:10:30) catalysts are listed in Table 2 including the positive peak potentials and corresponding peak current densities of ethanol electro-oxidation. Figure 6.b shows that the onset potentials of ethanol electro oxidation for Pt/C (100), Pt–Co/C (50:50), and Pt–Sn/C (50:50) are at about 300 mV vs. RHE. While for tri-metallic catalysts Pt–Sn–Co/C (60:30:10), Pt–Sn–Co/C (60:20:10) and Pt–Sn–Co/C (60:10:30) onset potential for ethanol electro-oxidation is earlier at about 200 mV vs. RHE, i.e. shifted to negative potential by 100 mV. The first electro-oxidation peak of ethanol on Pt–Sn/C (50:50) is at 823 mV (vs. Ag/AgCl), which is 75 mV higher than that of Pt–Sn–Ru/C (60:10:30). The current density at the first peak of ethanol electro-oxidation on Pt–Sn–Ru/C (60:10:30) is 16.9  $\text{mA}/\text{cm}^2$  which is higher than that on Pt–Sn/C (50:50) with a difference of 4.8  $\text{mA}/\text{cm}^2$ , but less than that of Pt–Sn–Co/C (60:20:20) and Pt–Sn–Ru/C

(60:30:10). The Pt–Sn–Co/C (60:30:10) shows highest peak current density (33.8 mA/cm<sup>2</sup>) at 803 mV peak potential, and hence possesses highest catalytic activity towards ethanol oxidation among all the catalysts prepared. Pt–Sn–Co/C (60:20:20) shows higher current density than Pt–Sn/C (50:50), Pt–Sn–Co/C (60:10:30) and Pt–Sn/C (50:50) catalysts, indicating that Pt–Sn–Co/C (60:20:20) is also a promising catalyst for ethanol electro-oxidation.

**Table 2 CV results of Pt/C, Pt–Co/C, Pt–Sn/C and Pt–Sn–Co/C electrocatalysts at room temperature.**

Catalyst	Scan rate 50 mV/s	
	Positive peak potential (mV vs. Ag/AgCl)	Peak current density (mA/cm <sup>2</sup> )
Pt/C (100)	795	8.5
Pt–Sn/C (50:50)	823	11.9
Pt–Co/C (50:50)	812	13.0
Pt–Sn–Co/C (60:10:30)	740	16.9
Pt–Sn–Co/C (60:20:20)	750	22.9
Pt–Sn–Co/C (60:30:10)	803	33.8

Pure Pt/C catalyst (Fig. 4b) does not behave as a very good anode for ethanol electro-oxidation due to its poisoning by strongly adsorbed intermediates such as CO<sub>ads</sub><sup>20</sup>. However, the introduction of Sn and Co promotes the electrocatalytic activity. In fact, as observed in Fig. 6b, the introduction of Sn and Co leads to an increase in the electro-activity of the binary and ternary electrocatalysts compared to pure Pt/C. The synergistic effect obtained with these elements can be explained by the activation of interfacial water molecules at lower potentials than in the case of pure Pt due to the presence of preferential sites for OH<sub>ads</sub> adsorption, as proposed in the case of Pt–Co for ethanol electro-oxidation. The presence of OH<sub>ads</sub> species in large amounts is necessary for the complete oxidation of poisoning intermediates such as CH<sub>x</sub> and CO<sup>15</sup>.

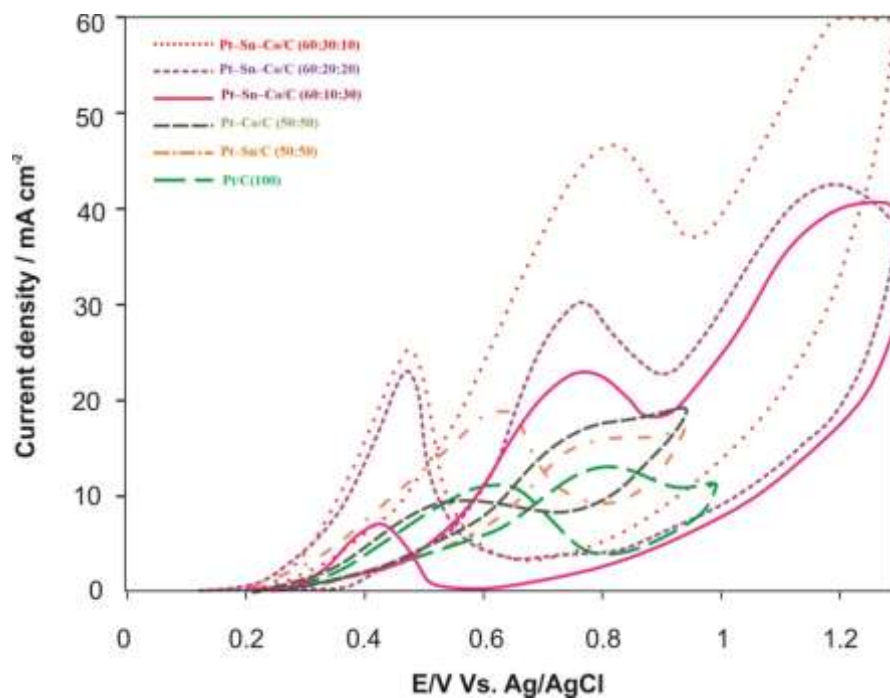


**Fig. 4b** Cyclic voltammety of Pt/C, Pt–Co/C, Pt–Sn/C and Pt–Sn–Co/C electrocatalysts in 0.5 M H<sub>2</sub>SO<sub>4</sub> and 1.0 M ethanol at room temperature with a scan rate of 50 mV/s.

The binary and ternary electrocatalysts performed better than Pt/C for ethanol oxidation. Moreover, when the binary electrocatalysts were compared to the ternary ones in terms of oxidation wave onset potential

and achieved current densities, the latter catalysts gave the best electrical performances. In the case of the ternary electrocatalysts, the best performance was achieved with lower Sn atomic ratios, which confirmed the previous results showing that low Sn atomic ratios (close to 10%) in bimetallic Pt–Sn electrocatalysts lead to higher activities towards ethanol oxidation<sup>21-23</sup>. On the other hand, addition of Co to Pt (Pt–Sn/C) had a little effect, whereas addition of Co to Pt–Sn greatly enhanced the electrocatalytic activity.

### 3.2.2. Chronoamperometry

Fig. 4.5 shows the current densities measured at a constant potential jumping from 0.05 to 1.0 V in 1.0 M ethanol+0.5 M H<sub>2</sub>SO<sub>4</sub>. The currents decay with time in a parabolic style and reach an apparent steady state within 80s. It can be seen that the current density of ethanol electrooxidation on the Pt<sub>60</sub>Sn<sub>30</sub>Co<sub>10</sub>/C catalyst is higher than that on the Pt<sub>60</sub>Sn<sub>20</sub>Co<sub>20</sub>/C, Pt<sub>60</sub>Sn<sub>10</sub>Co<sub>30</sub>/C, Pt<sub>50</sub>Sn<sub>50</sub>/C, Pt<sub>50</sub>Co<sub>50</sub>/C and Pt<sub>100</sub>/C catalyst at the same potentials. The activity change for ethanol oxidation decreases in the order of Pt<sub>60</sub>Sn<sub>30</sub>Co<sub>10</sub>/C > Pt<sub>60</sub>Sn<sub>20</sub>Co<sub>20</sub>/C > Pt<sub>60</sub>Sn<sub>10</sub>Co<sub>30</sub>/C > Pt<sub>50</sub>Sn<sub>50</sub>/C > Pt<sub>50</sub>Co<sub>50</sub>/C > Pt<sub>100</sub>/C, which is in fairly good agreement with our CV results. For the durability test, the chronoamperometric experiments were carried out at 0.05 to 1.0 V for 2000 s in the same conditions. Before each measurement, the solution was purged with high-purity nitrogen gas for at least 30 min to ensure oxygen-free measurements.

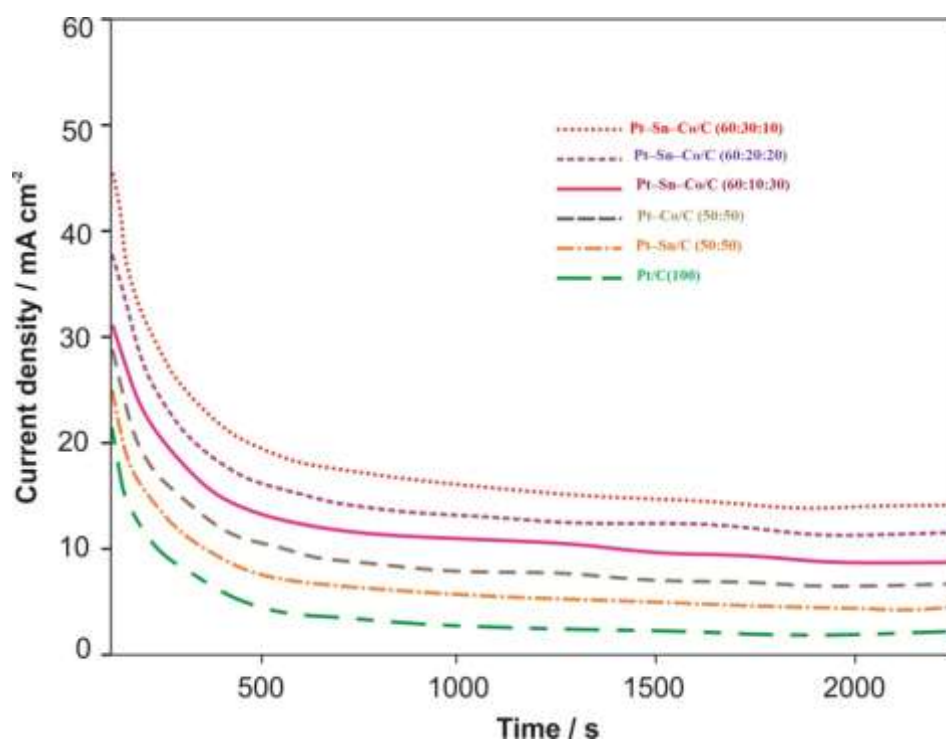
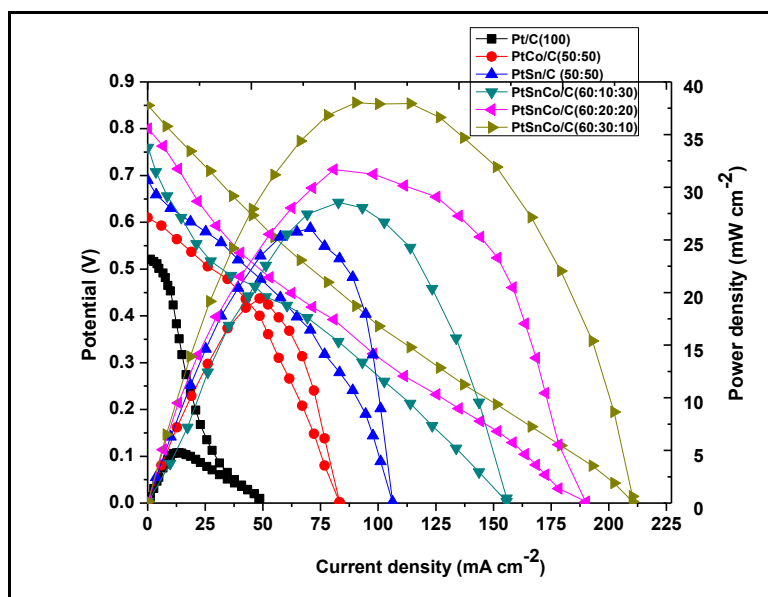


Fig. 5 CA of Pt<sub>60</sub>Sn<sub>30</sub>Co<sub>10</sub>/C, Pt<sub>60</sub>Sn<sub>20</sub>Co<sub>20</sub>/C, Pt<sub>60</sub>Sn<sub>10</sub>Co<sub>30</sub>/C, Pt<sub>50</sub>Sn<sub>50</sub>/C, Pt<sub>50</sub>Co<sub>50</sub>/C and Pt<sub>100</sub>/C electrocatalysts

### 3.3 Single cell performance

The microfluidic architecture of laminar flow-based membraneless fuel cells overcomes the fuel crossover and water management issues that plague membrane-based fuel cells (i.e., PEMFC, DEFC) and enables independent control of stream characteristics (i.e., flow-rate and composition)<sup>24-28</sup>. Here we focused on maximizing cell performance, in terms of power density, by tailoring various structural characteristics and catalytic activity of carbon supported ternary Pt–Sn–Co catalysts. A single cell performance was tested using Pt<sub>60</sub>Sn<sub>30</sub>Co<sub>10</sub>/C, Pt<sub>60</sub>Sn<sub>20</sub>Co<sub>20</sub>/C, Pt<sub>60</sub>Sn<sub>10</sub>Co<sub>30</sub>/C, Pt<sub>50</sub>Sn<sub>50</sub>/C, Pt<sub>50</sub>Co<sub>50</sub>/C and Pt<sub>100</sub>/C electrocatalysts as the anode. Polarization curves and power densities are shown in Fig. 6. For each catalyst, the open-circuit voltages (OCV) were different, as would be expected in onset potentials. The OCVs of Pt<sub>60</sub>Sn<sub>30</sub>Co<sub>10</sub>/C, Pt<sub>60</sub>Sn<sub>20</sub>Co<sub>20</sub>/C, Pt<sub>60</sub>Sn<sub>10</sub>Co<sub>30</sub>/C, Pt<sub>50</sub>Sn<sub>50</sub>/C, Pt<sub>50</sub>Co<sub>50</sub>/C are higher than that of Pt<sub>100</sub>/C, 0.52 V, and the order of OCV is exactly same as the onset potentials.



**Fig. 6** Polarization and power density curves of  $\text{Pt}_{60}\text{Sn}_{30}\text{Co}_{10}/\text{C}$ ,  $\text{Pt}_{60}\text{Sn}_{20}\text{Co}_{20}/\text{C}$ ,  $\text{Pt}_{60}\text{Sn}_{10}\text{Co}_{30}/\text{C}$ ,  $\text{Pt}_{50}\text{Sn}_{50}/\text{C}$ ,  $\text{Pt}_{50}\text{Co}_{50}/\text{C}$  and  $\text{Pt}_{100}/\text{C}$  electrocatalysts

The OCV of  $\text{Pt}_{60}\text{Sn}_{30}\text{Co}_{10}/\text{C}$  is the highest value of 0.85 V, which is approximately 0.33 V higher than that of  $\text{Pt}_{100}/\text{C}$ . This indicates that  $\text{Pt}_{100}/\text{C}$  is more rapidly poisoned by CO than any other alloy catalyst and that the oxidation of adsorbed CO is enhanced by the second or third metal. In the case of  $\text{Pt}_{60}\text{Sn}_{30}\text{Co}_{10}/\text{C}$  the overall performance is superior to that of the bimetallic electrocatalysts. The maximum power densities obtained for  $\text{Pt}_{60}\text{Sn}_{30}\text{Co}_{10}/\text{C}$ ,  $\text{Pt}_{60}\text{Sn}_{20}\text{Co}_{20}/\text{C}$ ,  $\text{Pt}_{60}\text{Sn}_{10}\text{Co}_{30}/\text{C}$ ,  $\text{Pt}_{50}\text{Sn}_{50}/\text{C}$ ,  $\text{Pt}_{50}\text{Co}_{50}/\text{C}$  and  $\text{Pt}_{100}/\text{C}$  are 37.9, 31.7, 28.6, 26.2, 18.8 and 6.  $\text{mW cm}^{-2}$ , respectively (Table 3). We conclude that the substitution of a small amount of Co for Sn aids in cleaning surfaces poisoned by CO and provides additional reaction sites for ethanol oxidation.

**Table 3** Summary of performance of single fuel cell tests using (2  $\text{mg cm}^{-2}$  catalyst loading, 40 wt% catalyst on carbon)

Anode catalysts	Open circuit Voltage (V)	Maximum power density ( $\text{mW cm}^{-2}$ )	Maximum current density ( $\text{mA cm}^{-2}$ )
$\text{Pt}_{100}/\text{C}$	0.52	6.0	48.3
$\text{Pt}_{50}\text{Co}_{50}/\text{C}$	0.61	18.8	85.1
$\text{Pt}_{50}\text{Sn}_{50}/\text{C}$	0.69	26.2	106.3
$\text{Pt}_{60}\text{Sn}_{10}\text{Co}_{30}/\text{C}$	0.76	28.6	155.7
$\text{Pt}_{60}\text{Sn}_{20}\text{Co}_{20}/\text{C}$	0.80	31.7	190.2
$\text{Pt}_{60}\text{Sn}_{30}\text{Co}_{10}/\text{C}$	0.85	37.9	210.3

In membraneless fuel cells, pure Pt/C catalyst does not behave as a very good anode for ethanol electro-oxidation due to its poisoning by strongly adsorbed intermediates such as CO. The binary and ternary electrocatalysts performed better than Pt/C for ethanol oxidation. Moreover, when the binary electrocatalysts were compared to the ternary ones in terms of oxidation the latter catalysts gave the best electrical performances. On the other hand, addition of Co to Pt (Pt–Co/C) had a little effect, whereas addition of Co to Pt–Sn greatly enhanced the electrocatalytic activity.

As mentioned in our previous studies<sup>29-40</sup>, the performance of the developed membraneless fuel cell enhanced profoundly if the concentration of oxidant in cathodic stream is 10 times larger, and the current density is also increased approximately ten times.

## 4 Conclusions

In this work, the study of ethanol oxidation on carbon-supported Pt–Sn–Co ternary nanoparticles has revealed details concerning the activity and stability of the catalysts in membraneless fuel cells. The maximum activity for ethanol oxidation was found for the Pt<sub>60</sub>Sn<sub>30</sub>Co<sub>10</sub>/C than the Pt<sub>60</sub>Sn<sub>20</sub>Co<sub>20</sub>/C, Pt<sub>60</sub>Sn<sub>10</sub>Co<sub>30</sub>/C, Pt<sub>50</sub>Sn<sub>50</sub>/C, Pt<sub>50</sub>Co<sub>50</sub>/C and Pt<sub>100</sub>/C. The significantly enhanced catalytic activity for ethanol oxidation can be attributed to the high dispersion of ternary catalysts and to Co acting as a promotion agent. XRD results show the homogenous alloy structure of Pt, Sn and Co. The TEM images indicated an average size of ternary nanoparticles of 3-4 nm. The atom ratio of Pt, Sn and Co from EDX analyses is close agreement with the original precursor concentration. The composition of ternary nanoparticles can be conveniently controlled by adjusting the initial metal salt solution and preparation conditions. The electrochemical experiments showed that the Pt<sub>60</sub>Sn<sub>30</sub>Co<sub>10</sub>/C nanoparticles have higher catalytic activity than that of the other catalysts. We expect that the MLEFC may be a promising candidate for practical fuel cells to establish a clean and sustainable energy future. Further work is necessary to characterize the catalysts using different surface analysis techniques and to conduct tests of these electrocatalysts in microfluidic membraneless fuel cells.

## 5. References

1. Kiruthika S and Rajesh M. P., Synthesis and Characterization of Pd–Ir–Ni/C Electrocatalysts for Ethanol Oxidation in Membraneless Fuel Cells, *International Journal of ChemTech Research*, 7, 2015, pp 3148-3154.
2. Nayeemunisa S.M, Kiruthika S and Muthukumar B, Electro-oxidation of Isopropanol in Membraneless Fuel Cells, *International Journal of ChemTech Research*, 7, 2015, pp 3057-3062.
3. Niranjana S.R.J and Vashantha R, Development of Novel anode catalysts for Membraneless Sodium Perborate Fuel cells, *International Journal of ChemTech Research*, 7, 2015, pp 3051-3056.
4. Priya M and Muthukumar B, Enhanced Performance an Ethanol Membraneless Fuel Cell in Acidic Medium, *International Journal of ChemTech Research*, 7, 2015, pp 3026-3032.
5. Adamson KA, Pearson P, Hydrogen and methanol: a comparison of safety, economics, efficiencies and emissions, *J. Power Sources*, Vol.86, p.548, 2000.
6. McNicol BD, Rand DAJ, Williams KR, Direct methanol-air fuel cells for road transport, *J. Power Sources*, Vol.83, p.15, 1999.
7. Hart D, Leach MA, Fouquet R, Pearson PJ, Bauen A, Methanol infrastructure - will it affect the introduction of SPFC vehicles?, *J. Power Sources*, Vol.86, p.542, 2000.
8. Kiso F, Arashi N, Hybrid Methanol-Production Process, *Applied Energy*, Vol.59, p.215, 1998.
9. Beden B, Lamy C, Bewick A, Kunimatsu K, Electrosorption of carbon monoxide on platinum single crystals in perchloric acid medium, *J. Electroanal. Chem.* Vol.121, p.343, 1981.
10. Hamnett A, Mechanism and electrocatalysis in the direct methanol fuel cell. *Catalysis Today*, Vol.38, p.445, 1997.
11. Burnstein GT, Barnett CJ, Kucernak AR, Williams KR, Aspects of the anodic oxidation of methanol, *Catalysis Today*, Vol.38, p.425, 1997.
12. Chan KY, Ding J, Ren J, Cheng S, Tsang KY, Supported Mixed Metal Nanoparticles for Fuel Cell Electrode, *J. Mater. Chem.*, Vol.14, p.505, 2004.
13. Rivera EC, Volpe DJ, Alden L, Lind C, Downie C, Vazquez-Alvarez T, Electrocatalytic Activity of Ordered Intermetallic Phases for Fuel Cell Applications, *J. Am. Chem. Soc.*, Vol.126, p.4043–4049, 2004.
14. Xiong L, Kannan A, Manthiram A, Pt-M (M = Fe, Co, Ni and Cu) electrocatalysts synthesized by an aqueous route for proton exchange membrane fuel cells, *Electrochem. Commun.*, Vol.4, p.898–903, 2002.
15. Gasteiger HA, Markovic N, Ross PN, Cairns EJ, Methanol electrooxidation on well-characterized Pt-Ru alloys, *J. Phys. Chem.*, Vol.97, p.12020–12029, 1993.
16. Yajima T, Uchida H, Watanabe M, In-situ ATR-FTIR spectroscopic study of electro-oxidation of methanol and adsorbed CO at Pt-Ru alloy, *J. Phys. Chem. B.* Vol.108, p.2654–2659, 2004.
17. Moreno B, Jurado JR, Chinarro E, Pt-Ru-Co catalysts for PEMFC synthesized by combustion, *Catalysis Communications*, Vol.11, p.123–126, 2009.
18. Ahn SH, Kwon OJ, Kim SK, Choi I, Kim JJ, Electrochemical preparation of Pt-based ternary alloy catalyst for direct methanol fuel cell anode, *Int. J. of Hydrogen Energy*, Vol.35, p.13309–13316, 2010.

19. Ribeiro J, dos Anjos DM, Kokoh KB, Countanceau C, Leger JM, Olivi P, de Andrade AR, Tremiliosi-Filho G, Carbon-supported ternary PtSnIr catalysts for direct ethanol fuel cell, *Electrochim. Acta*. Vol.52, p.6997, 2007.
20. Pechini PM, Method of preparing lead and alkaline earth titanates and niobates and coating method using the same to form a capacitor, *Unites States Patent Office*, 3330697, 1967.
21. Selvarani V, Kiruthika S and Muthukumar B, Performance of Pt-based Anode Catalyst for Urea Electro-Oxidation in Membraneless Fuel Cells, *International Journal of ChemTech Research*, 7, 2015, pp 3069-3074.
22. Thilagaand S and Muthukumar B, Electrocatalysis of Oxygen Reduction on Carbon Supported Platinum Catalysts in Membraneless Fuel Cells, *International Journal of ChemTech Research*, 7, 2015, pp 3141-3147.
23. Vijayaramalingam K, Kiruthika S, Muthukumar B, Electrochemical Oxidation of Platinum Based Anode Catalysts for Membraneless Fuel Cells, *International Journal of ChemTech Research*, 7, 2015, pp 3063-3068.
24. Shree Devi S, Krishnamoorthy P and Muthukumar B, Iron(II) catalysis in perborate oxidation of 5-oxo acids, *International Journal of ChemTech Research*, 7, 2015, pp 2902-2910.
25. Durga S and Muthukumar B, Electrooxidation of Hydrazine using H<sub>2</sub>O<sub>2</sub> as An Oxidant in Membraneless Fuel Cells, *International Journal of ChemTech Research*, 7, 2015, pp 3134-3140.
26. Bonesi A, Asteazaran M, Moreno MS, Zampieri G, Bengio S, Triaca W, Castro Luna AM, Preparation and evaluation of carbon-supported catalysts for ethanol oxidation, *J. Solid State Electrochem.* Vol.17, p.1823, 2013.
27. Ribeiro J, dos Anjos DM, Kokoh KB, Coutanceau C, Leger J-M, Olivi P, de Andrade AR, Tremiliosi-Filho G (2007) Carbon-supported ternary PtSnIr catalysts for direct ethanol fuel cell, *Electrochimica Acta* 52:6997–7006.
28. Choi WC, Woo SI, *J. Power Sources*. Vol.124, p.420–425, 2003.
29. Jerine Peter Simon, Kadar Basha Shalluddin, Giridharan Ramalingam, Gunaseelan D, Evan Prince Sabin, Patterns of interaction of major active components of the blue green algae *Spirulina fusiformis* against chosen orphan nuclear receptors: an in silico study, *International Journal of ChemTech Research* Vol.9, No.04 pp 675-682, 2016.
30. A.Vanaja, K.Srinivasa Rao, Influence of Precursors on Structural and Optical Properties of ZnO Nanopowders Synthesized in Hydrolysis medium *International Journal of ChemTech Research*, Vol.9, No.04 pp 691-698, 2016.
31. R.R.Muthuchudarkodi, S. Kalaiarasi, Synthesis, Electrochemical Characterization Of MoO<sub>3</sub>-CeO<sub>2</sub> Mixed Oxide Nano Particles, *International Journal of ChemTech Research*, Vol.9, No.04 pp 699-706, 2016.
32. Yegireddi Shireesha, Bade Venkata Suresh, P Govinda Rao, Emissions Reduction using Catalyst Converter, *International Journal of ChemTech Resear* Vol.9, No.03 pp 540-549, 2016.
33. Ferial Zaher, M.S.Gad, Assessment of Biodiesel Derived from Waste Cooking Oil as an Alternative Fuel for Diesel Engines, *International Journal of ChemTech Research*, Vol.9, No.03 pp 140-146, 2016.
34. K Prasada Rao, K Santarao, P Govinda Rao, Experimental Investigation on Performance and Emission Characteristics of a DI Diesel Engine Fuelled With Rice Bran Oil Methyl Ester And Methanol as an additive, *International Journal of ChemTech Research*, Vol.9, No.03 pp 258-266, 2016.
35. P.A.Jeeva, S. Narayanan, S.Karthikeyan, A review on Black coatings for Solar Energy Storing Systems, *International Journal of ChemTech Research* Vol.9, No.03 pp 589-596, 2016.
36. T. Baskar, K.S.Rajni, Effect of different Sulfur concentration on structural and magnetic properties of electrodeposited NiCoS magnetic thin films, *International Journal of ChemTech Research*, Vol.9, No.04 pp 317-324, 2016.
37. Foad S. Hashim, Mohammad H. Almaamori, Farah J. Hamood, Effect of Silica on the Mechanical Properties of Rubber Reclaim Composite, *International Journal of ChemTech Research*, Vol.9, No.04 pp 325-333, 2016.
38. P.Ramesh Babu, Ravishanker Babu, Starch assisted sol gel syntheses and characterization of NdFeO<sub>3</sub>, *International Journal of ChemTech Research*, Vol.9, No.04 pp 364-369, 2016.
39. Vigier F, Coutanceau C, Hahn F, Belgsir EM, Lamy C (2004) On the mechanism of ethanol electro-oxidation on Pt and PtSn catalysts: electrochemical and in situ IR reflectance spectroscopy studies. *J Electroanal. Chem.* 563:81-89.

40. Lamy C, Rousseau S, Belgsir E, Coutanceau C, Léger J-M (2004) Recent progress in the direct ethanol fuel cell: development of new platinum–tin electrocatalysts. *Electrochim Acta* 49:3901–3908. Doi:10.1016/j.electacta.2004.01.078.

\*\*\*\*\*